Design of an Adaptive Flux Observer for Sensorless Switched Reluctance Motors Using Lyapunov Theory

Hady ABDELMAKSOUD[1,2], Mohamed ZAKY[1,2]
[1]*Electrical Engineering Department, Faculty of Engineering, Menoufia University, Shebin El-Kom 32511, Egypt*
[2]*Electrical Engineering Department, Faculty of Engineering, Northern Border University, Arar 1321, Kingdom of Saudi Arabia*
mszaky78@yahoo.com

Abstract—**This paper proposes an adaptive flux observer for a sensorless switched reluctance motor. The observer adaptive gains are designed using the Lyapunov theory to guarantee both the accuracy and stability of the sensorless control of a switched reluctance motor. A nonlinear inductance model is developed based on a finite element analysis data and used in the estimation algorithms for rotor position and speed. The adaptive flux observer estimates the rotor position at low, medium, and high speeds. A low-frequency ramp method is proposed to excite the switched reluctance motor during standstill where the voltage and current signals are unobservable. The proposed hybrid method is characterized by simplicity, accuracy, ease of implementation, and low real-time computation burden. Therefore, the sensorless control technique depends only on active phase measurements without extra hardware and memory storage for real-time implementation. Complete sensorless control of a three-phase 6/4-pole switched reluctance motor drive system is carried out using Matlab/Simulink. Also, it is implemented experimentally in real-time using the digital signal processor-DS1102 control board. The simulation and experimental results of the proposed sensorless scheme demonstrate the accurate estimation of both the speed and rotor position during the transient and steady states.**

Index Terms—**AC machines, Lyapunov methods, motor drives, observers, state estimation.**

I. Introduction

The switched reluctance motor (SRM) has become an attractive candidate for various applications, due to its simple structural, low-cost, and robustness [1-2]. The continuous and the precision knowledge of the rotor position for SRM is essential for the improvement of its performance. Traditionally, mechanical position instruments have been used in SRM drives to sense the rotor location. Nevertheless, complexity and high cost are the main drawbacks that limit the adoption of position instruments, especially at high speeds [3-5]. Critical solution is to advance sensorless control or self-sensing methods to overcome these problems. For the sensorless control of SRM, there are two basic methodologies of position estimation techniques: active probing and nonintrusive estimation methods. Active probing methods are based on a pulse injection mechanism. Therefore, these methods are effective at low speeds. Alternatively, nonintrusive estimation methods depend on the machine mathematical model, and efficiently estimate the rotor position at high speeds [6-10].

Torque ripple minimization with sensorless observer was introduced in [11] where a sliding mode observer was used. It gives a good estimation at high speeds, but the error was relatively large at low speed and starting.

A general nonlinear magnetization model was proposed in [12] to predict the rotor position at very high speed; however, plenty of problems are remained at low speeds. Position estimation at starting and low speed was introduced in [13, 14] using pulse injection strategy. A series of initial position detection methods were presented in [15] using phase inductance coordinate transformations. This method is not appropriate for high load and high speed driving–running conditions.

Recently, the intelligence algorithms as artificial neural networks (ANN), fuzzy logic have been employed [16-18]. In [19], a fuzzy logic based motor model was reported, wherein a large number of fuzzy rules were involved to estimate the rotor position. In [20], an ANN was applied for identification of the rotor position for SRM. However, this technique needs priori magnetization data and a large amount of calculations.

The hybrid sensorless algorithms, one for low speed and the other for high speed, have been appeared lately in the publications [21-23]. A hybrid sensorless controller was integrated in [24] to estimate the rotor position along entire speed range. A discrete sensor was utilized for low speeds along with sliding mode observer for high speeds. A DC pulse was applied to the stator winding for a short time to detect the rotor position at starting [25], and a second algorithm based magnetic characteristics was designed to identify the rotor position at running. The pulse injection together with observer was integrated in [26, 27] to estimate the rotor position over entire speed range. In [28], rotor position is initially calculated based on the flux linkage-position-current characteristics while two techniques have been operated sequentially at low and high speeds. For the sensorless direct torque control, detection of maximum and minimum inflection points of the phase inductance was proposed in [29]. The scheme not only requires start up algorithm but also doesn't provide continuous information of the rotor position. A position estimation method based on

Digital Object Identifier 10.4316/AECE.2020.02014

variable coefficient linear inductance model was studied in [30] to reduce the saturation effect.

Briefly, Most of hybrid sensorless techniques apply injection pulses to the idle phase for determination the rotor position at standstill. These pulses not only need additional circuits, but also lead to reliability problems [31, 32].

This paper proposes a novel feedback gain design of adaptive flux observer (AFO) for a sensorless SRM. The finite element (FE) analysis and a nonlinear inductance model are first presented. Then, the dynamic model of SRM is defined. The AFO for estimation of both the rotor position and speed is derived using the proposed nonlinear mathematical model of the SRM. The observer adaptive gains are designed based on Lyapunov theory to guarantee both good performance and stable operation. The rotor position estimation problem of sensorless SRM at standstill and very low speed is solved using a low frequency ramp method. The complete sensorless control of SRM drive system using the proposed hybrid estimation method is carried out by computer simulation. Moreover, it is implemented in the laboratory using DSP-DS1102, an asymmetric half-bridge inverter, and a three-phase 6/4 SRM. Different simulation and experimental results under various working conditions are presented to verify the validity of the proposed design.

II. Dynamic SRM Model

To maximize the energy conversion of SRM, it is generally worked in the magnetically saturated mode. A proper modeling of the nonlinear flux–current–angle (λ, i, θ) characteristics of the SRM is required to take into consideration the magnetic nonlinearities. A three-phase 6/4 SRM (six stator teeth, four rotor teeth) is utilized to validate the proposed model. The SRM data is given in Table I in the appendix. Firstly, the magnetic circuit of 6/4 SRM is analyzed using the finite element method. The obtained results of FE analysis are used to derive a simplified inductance model for SRM.

A. FE Analysis

In this section, a two-dimensional FE is utilized to analyze the magnetic circuit. The magnetic field of SRM can be described using the magnetic vector potential Az as expressed by (1).

$$\frac{\partial}{\partial x}(\nu\frac{\partial A_z}{\partial x})+\frac{\partial}{\partial y}(\nu\frac{\partial A_z}{\partial y})+J=0 \quad (1)$$

where,

ν is the magnetic reluctivity of the material.

J is the induced current density.

Applying the finite element numerical solution of (1), the magnetic circuit can be analyzed from the unaligned position ($\theta = 0^o$) up to the aligned position ($\theta = 45^o$) under different phase current values. Fig. 1 shows a flux distribution for the 3-phase 6/4 SRM. The inductance-angle curves at different phase current values are presented in Fig. 2.

B. Nonlinear Inductance Model

To calculate the nonlinear inductance model, the flux linkage equation is introduced for phase k as given in (2).

$$\lambda_k(i_k,\theta)=L_k(i_k,\theta)i_k \quad (2)$$

where, L_k is the self-inductance of phase k.

Then, L_k is derived from (2) as follows:

$$L_k(i_k,\theta)=\frac{\lambda(i_k,\theta)}{i_k} \quad (3)$$

This equation of L_k is considered the key input to the proposed model. Using the data of both the flux linkage and phase current obtained from FE analysis, a computer program is built to calculate L_k as a function of phase current and position angle. The resultant data is programmed and simulated to plot the inductance-angle curves at different values of phase current as presented in Fig. 2.

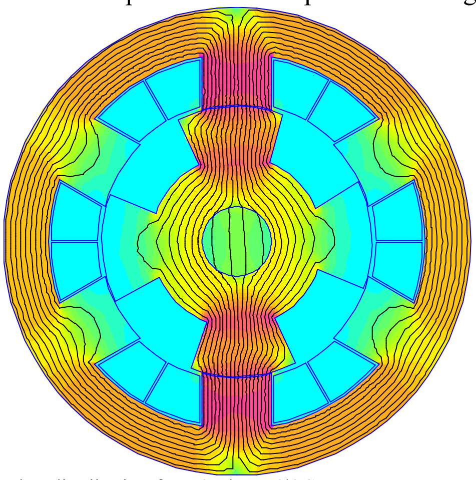

Figure 1. Flux distribution for a 3-phase 6/4 SRM

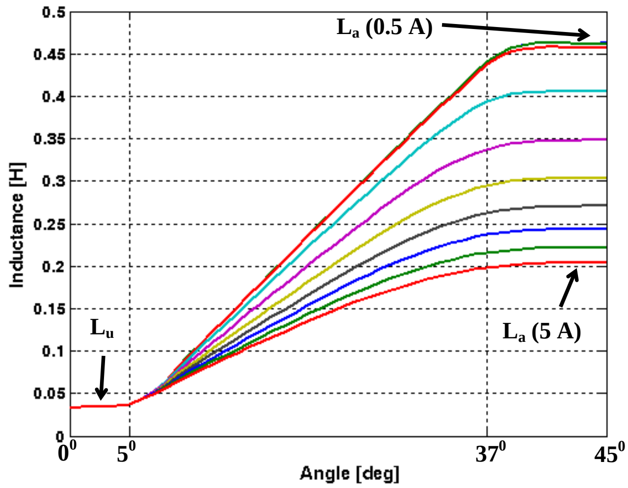

Figure 2. Inductance-angle curves at different values of phase current

The phase inductance can be described by a set of trapezoidal curves as shown in Fig. 2; its bottom value is constant at L_u and the top value is L_a which varies with phase current. So, it can be characterized as follows:

$$L_k(i_k,\theta_k)=\begin{cases} L_u & \theta_1\le\theta\le\theta_2 \\ L_u+m\theta_k & \theta_2\le\theta\le\theta_3 \\ L_a & \theta_3\le\theta\le\theta_4 \end{cases} \quad (4)$$

where,

$$m=\frac{L_a-L_u}{\beta_S} \quad (5)$$

β_S is the stator pole arc, $\theta_1=0^o$, $\theta_2=5^o$, $\theta_3=37^o$ and $\theta_4=45^o$. It is found that L_k is varied with the phase current and can be represented by a second order polynomial equation using (6).

$$L_k=b_0 i_k^2+b_1 i_k+b_2 \quad (6)$$

The constants b_0, b_1, and b_2 are calculated by the curve fitting method. Their values are given in Table II in the appendix.

To verify the accuracy of the proposed model introduced above, the flux linkage-current-rotor position characteristics obtained from a FE analysis were compared with those generated from the proposed inductance model [33].

The basic torque equation is given by

$$T = \frac{1}{2} i^2 \frac{dL}{d\theta} \tag{7}$$

Then, the phase torque equation is determined by substituting (4) into (7) as follows:

$$T_k = \begin{cases} 0 & \theta_1 \le \theta \le \theta_2 \\ \frac{1}{2} i_k^2 m & \theta_2 \le \theta \le \theta_3 \\ 0 & \theta_3 \le \theta \le \theta_4 \end{cases} \tag{8}$$

The total developed torque can be calculated by summing the instantaneous torque developed by all phases.

$$T = \sum_{k=1}^{q} T_k\left(\theta_k, i_k\right) \tag{9}$$

C. Dynamic Model of SRM

The dynamic model of SRM can be described using (10) - (12) as follows:

$$\frac{di_k}{dt} = \frac{1}{L_k}(V_k - i_k R_k - i_k \omega \frac{dL_k}{d\theta}) \tag{10}$$

$$\frac{d\theta}{dt} = \omega \tag{11}$$

$$\frac{d\omega}{dt} = \frac{1}{J}(T - T_L - B\omega) \tag{12}$$

where,

V_k is the phase voltage.
i_k is the phase current.
R_k is the phase resistance.
L_k is the phase inductance.
ω is the rotor speed,
θ is the rotor position.
J is the moment of inertia
B is the viscous damping constant.
T is the motor developed torque.
T_L is the load torque.

III. Adaptive Flux Observer

A. AFO Model

The AFO is one of the machine model based methods of state estimation. It is utilized with a state-space model of the SRM to estimate rotor position and speed from phase voltage and current signals. The estimation procedures can be systemically arranged in the following steps.

Firstly, the actual flux is calculated from motor terminal measurements using the phase voltage equation as given in (13). The actual flux is independent of the rotor position and speed. Then, the estimated flux from the mathematical SRM model depends on the estimated inductance and phase current as in (14). It is dependent on the rotor position and speed.

$$\lambda_k(t) = \int_0^t \{V_k(t) - Ri_k(t)\}dt \tag{13}$$

$$\hat{\lambda}_k(t) = \hat{L}(i_k, \hat{\theta}) * i_k \tag{14}$$

The error function e_f depends on the measured and estimated rotor flux as given (15). The function $f_k'(\hat{\theta})$ is chosen to guarantee that the error e_f forces the estimated rotor position to converge to motoring or generating mode.

$$e_f = \sum_{k=1}^{N_{ph}} f_k'(\hat{\theta})(\lambda_k - \hat{\lambda}_k) \quad \text{with } f_k'(\hat{\theta}) = \left.\frac{df_k(\hat{\theta})}{d\theta}\right|_{\theta=\hat{\theta}} \tag{15}$$

In this paper, the following function is introduced:

$$f_k(\hat{\theta}) = \cos(N_r\hat{\theta} - (k-1) * 2\pi / q) \tag{16}$$

where, N_r is the number of rotor poles and q is the number of SRM phases.

The AFO is constructed to estimate both the rotor position and speed by comparing the actual and estimated fluxes. The flux error between the actual and estimated fluxes is derived. The rotor position and speed are estimated using (17) and (18).

$$\frac{d\hat{\theta}}{dt} = \hat{\omega} + k_p e_f(t) \tag{17}$$

$$\hat{\omega} = k_s \int e_f(t)dt \tag{18}$$

where,

$\hat{\theta}$ is the estimated rotor position
$\hat{\omega}$ is the estimated speed
e_f is an error function based on measured and estimated variables.
k_p is the position adaptive gain
k_s is the speed adaptive gain.

The observer error dynamics of (19) and (20) are introduced using the estimated position and speed errors as follow:

$$e_p(t) = \theta(t) - \hat{\theta}(t) \tag{19}$$

$$e_s(t) = \omega(t) - \hat{\omega}(t) \tag{20}$$

The derivative of (19) gives

$$\frac{de_p}{dt} = \frac{d\theta}{dt} - \frac{d\hat{\theta}}{dt} \tag{21}$$

Using (11), (17), and (20), the derivative of estimated position error becomes,

$$\frac{de_p(t)}{dt} = \omega(t) - \hat{\omega}(t) - k_p e_f(t) = e_s(t) - k_p e_f(t) \tag{22}$$

The derivative of (20) gives,

$$\frac{de_s(t)}{dt} = \frac{d\omega}{dt} - \frac{d\hat{\omega}}{dt} \tag{23}$$

Using (12) and (18), the derivative of estimated speed error yields

$$\frac{de_s(t)}{dt} = \frac{1}{J}\left(T - T_L - B\omega(t)\right) - k_s e_f(t) \tag{24}$$

B. Design of Observer Adaptive Gains

To design the adaptive gains for a stable AFO, Lyapunov stability theory is applied.

Proof 1: The Lyapunov function is chosen as (25).

$$V_s(t) = \frac{1}{2} e_s^2(t) \tag{25}$$

Differentiate (25) yields:

$$\begin{aligned} \dot{V}_s(t) &= e_s(t)\dot{e}_s(t) \\ &= e_s(t)\left(\frac{1}{J}\left(T - T_L - B\omega(t)\right) - k_s e_f(t)\right) < 0 \end{aligned} \tag{26}$$

The sufficient conditions of stability according to Lyapunov theory can be ensured only when $\dot{V}_s(t)$ is a negative definite. Consequently, the gain k_s is selected to be large enough such that $\dot{V}_s(t)$ is a negative definite as shown in (27).

$$k_s > \frac{1}{e_f(t)}\left(\frac{1}{J}\left(T - T_L - B\omega(t)\right)\right) \tag{27}$$

$$k_s = l_1 \cdot \frac{1}{e_f(t)}\left(\frac{1}{J}\left(T - T_L - B\omega(t)\right)\right) \tag{28}$$

where, l_1 is a positive number.

Proof 2: The Lyapunov function is chosen as (29).

$$V_p(t) = \frac{1}{2} e_p^2(t) \tag{29}$$

Differentiate (29) yields:

$$\dot{V}_p(t) = e_p(t)\dot{e}_p(t) = e_p(t)\left(e_s(t) - k_p e_f(t)\right) < 0 \tag{30}$$

The sufficient conditions of stability according to Lyapunov theory can be ensured only when $\dot{V}_p(t)$ is a negative definite. Consequently, the gain k_p is selected to be large enough such that $\dot{V}_p(t)$ is a negative definite as shown in (31).

$$k_p > \frac{e_s(t)}{e_f(t)} \tag{31}$$

$$k_p = l_2 \cdot \frac{e_s(t)}{e_f(t)} \tag{32}$$

where l_2 is a positive number.

To ensure the observer stability and good dynamic performance, the adaptive gains k_p and k_s should be properly designed. The gains l_1 and l_2 are considered safety factors of the AFO and should be selected enough to fulfill the limited conditions of (27) and (31), respectively. This guarantees the observer stability.

To show the estimation procedures of rotor position and speed from the phase voltages and currents, the block diagram in Fig. 3 presents the parallel estimation of the rotor flux, speed, and rotor position.

IV. Simulation Results

The speed and rotor position estimation algorithms in the abovementioned analysis are executed in the Matlab/Simulink software. This is to verify their accuracy and robustness. Various simulation results are presented.

A. Starting Operation

The performance of the sensorless control of SRM during the starting operation is shown in Fig. 4. This figure presents the estimated and actual speeds as well as the estimated speed error. The SRM starts up from standstill to a speed of 700 rpm. It is obvious that the estimated speed precisely tracks the actual speed.

B. Step Speed Change

The performance of the sensorless control of SRM is also tested during step speed change to evaluate the proposed AFO feedback gains as well as the speed controller. The simulation results of actual and estimated speeds as well as estimated speed error during step speed change from 550 rpm to 1100 rpm are presented in Fig. 5. Also, the simulation results of actual and estimated speeds as well as estimated speed error during step speed change from 1000 rpm to 450 rpm are shown in Fig. 6. The estimated speed has a good convergence with the actual speed. It is evident that the estimated speed error has a small value and decays to zero rapidly.

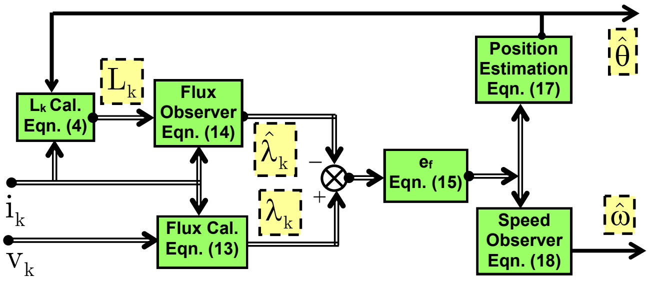

Figure 3. Block diagram of the parallel estimation of the rotor flux, speed, and rotor position

C. Rotor Position Estimation

Fig. 7 present the comparison between the actual and estimated rotor positions as well as the estimated position error at speed 500 rpm, respectively. It is clear that the rotor position is estimated accurately when compared with the actual rotor position.

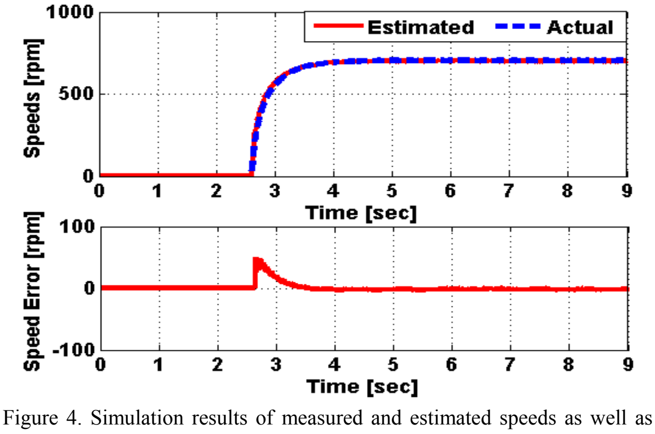

Figure 4. Simulation results of measured and estimated speeds as well as estimated speed error during starting operation at 700 rpm

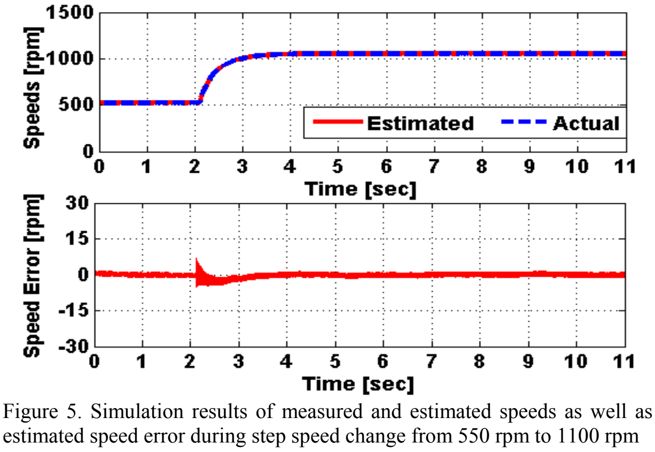

Figure 5. Simulation results of measured and estimated speeds as well as estimated speed error during step speed change from 550 rpm to 1100 rpm

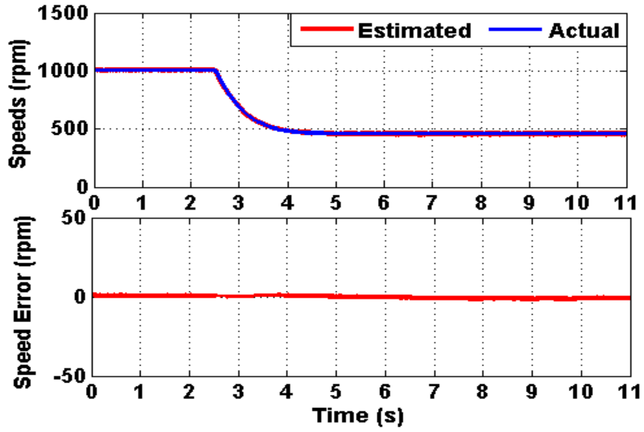

Figure 6. Simulation results of measured and estimated speeds as well as estimated speed error during step speed change from 1000 rpm to 450 rpm

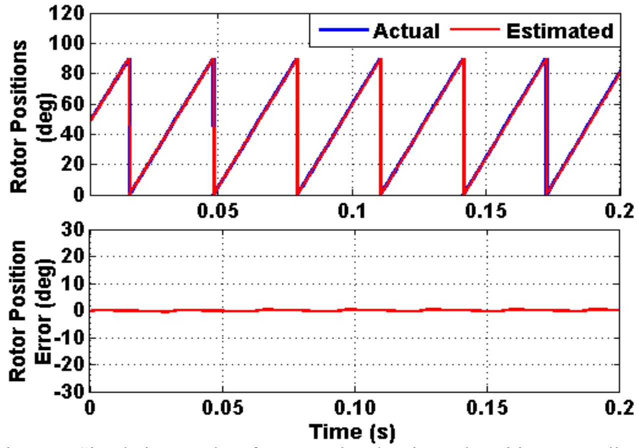

Figure 7. Simulation results of measured and estimated positions as well as estimated position error at speed of 500 rpm

V. Implementation Of The Sensorless SRM Drive System

A. Laboratory System Implementation

The proposed design of AFO for rotor position and speed estimations, as shown in Fig. 3, is verified by experimental tests. Fig. 8 presents the schematic diagram of the complete sensorless control of SRM drive system. A 3-phase 6/4 SRM is utilized. The machine data and rating are given in the appendix. An asymmetric three-phase half-bridge inverter is employed to excite the SRM. The gate drive circuits as well as interface circuits are built in the laboratory. Current and voltage transducer circuits are used to measure the voltage and current signals. These measured signals are sent to the digital signal processor (TMS320C31) of the DS-1102 control board using analog to digital converters.

The rotor position and speed estimators are built using Matlab/Simulink software. The reference speed is compared with the estimated speed. The resultant error is treated with the speed controller. The torque command is converted to the reference current signals. These reference currents are compared to the measured currents according to the position angle using the current regulator and PWM generation signals are created. These PWM signals are generated and passed through digital output ports to opto-isolators and then, to inverter gate drivers. An encoder with 500 pulse/revolution is employed for the purpose of verification with the estimated speed.

B. Zero Speed Operation of Sensorless SRM

In the proposed AFO, the rotor position and speed are estimated based on the measured voltage and current signals only. Model-based methods using AFO for state estimation are relatively simple, low computation burden, and low cost in comparison to sensorless methods using pulse injection. However, they require precise mathematical model. Moreover, they have a major challenge during starting operation at zero speed. This is because that the machine variables at zero speed are unobservable. Therefore, it is difficult to estimate the rotor position and speed at zero speed. Also, the model-based sensorless methods using flux estimation at very low speeds have a speed estimation error due to integration error.

In this paper, a novel simple method in conjunction with AFO is proposed to solve the challenge of model-based methods for speed estimation at zero speed and very low speeds. This method uses frequency ramp at zero speed where the voltage and currents are unobservable. It depends on applying low frequency ramp function that is similar to the rotor position response at very low speed as a source of rotor position angle as shown in Fig. 9 (a). It can be observed that it has been rested every 90^{o} equal to the rotor pole pitch. Based on this ramp function, a train of sequence pulses are generated and supplied the gate drive circuit. The inverter receives these sequence pulses through the gate drive circuit and applies a dc voltage on the stator winding. Therefore, the SRM starts from standstill as a stepper motor. This allows extracting information from the response of the system. The frequency of the ramp function is chosen such that it allows transferring the excitation from phase to another as shown in Fig. 9(b). When the SRM rotates, the integration issue of the flux observer at very low speeds is solved. So, the AFO works well and ensures good rotor position and speed estimations. The proposed approach uses AFO for rotor position and speed low, medium and high speeds, and ramp estimation method is used only at zero and very low speeds. Fig. 10 shows a flow chart of transition algorithm for zero-sensorless operation during standstill to AFO method at low and high speeds.

C. Experimental Results

Various experimental results are captured at different operating conditions to verify the accuracy and convergence of the sensorless control of SRM. Fig. 11 shows the experimental results of phase voltage and phase current. The estimated rotor flux is presented in Fig. 12.

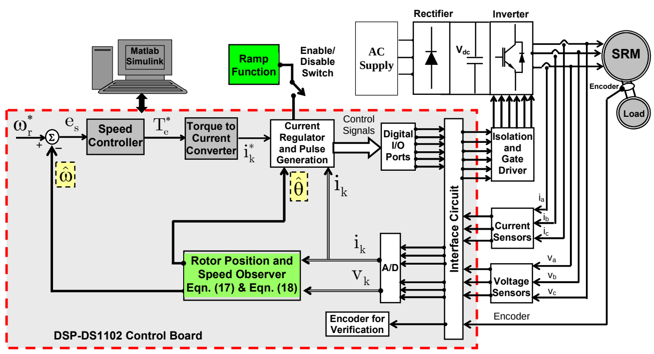

Figure 8. Schematic block diagram of the sensorless control of SRM drive system using AFO

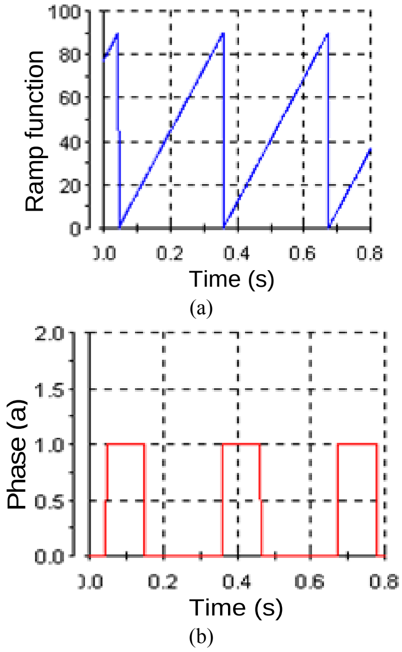

Figure 9. (a) Low frequency ramp function. (b) The excitation pulses during standstill

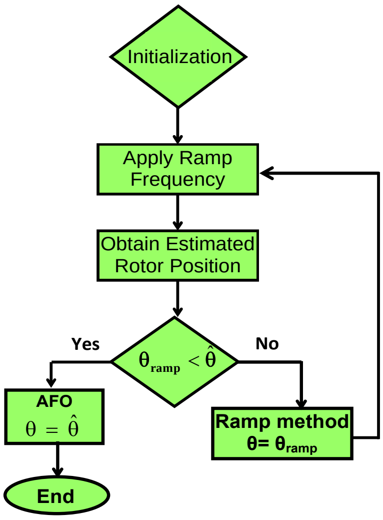

Figure 10. Flow chart of transition algorithm for zero-sensorless operation during standstill

The estimated speed and rotor position using the AFO are compared with their actual values. In Fig. 13, the performance of the sensorless control of SRM during the starting operation is presented. This figure presents the estimated and actual speeds as well as the estimated speed error. The SRM starts up from standstill to a speed of 700 rpm. It is obvious that the estimated speed precisely tracks the measured speed. The estimated speed error rapidly decays to a very small value around zero.

The performance of the sensorless control of SRM is also tested during step speed change to evaluate the proposed AFO feedback gains as well as the speed controller. The experimental results of measured and estimated speeds as well as estimated speed error during step speed change from 550 rpm to 1100 rpm are presented in Fig. 14. Also, the experimental results of measured and estimated speeds as well as estimated speed error during step speed change from 1000 rpm to 450 rpm are shown in Fig. 15. The estimated speed has a good convergence with the measured speed. It is evident that the estimated speed error has a small value and decays to zero rapidly. Also, it is observed that the speed controller works well. As shown, the measured and estimated speeds track the reference speed smoothly. These tests prove the robustness of the proposed AFO and the speed controller of the sensorless control of SRM.

Fig. 16 and Fig. 17 present the comparison between the measured and estimated rotor positions as well as the estimated position error at speed 500 rpm and 700 rpm, respectively. It is clear that the rotor position is estimated accurately when compared with the measured rotor position.

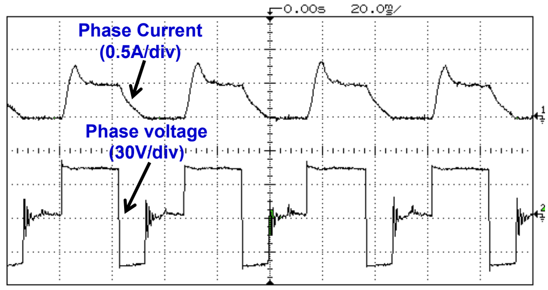

Figure 11. Experimental results of phase voltage and phase current

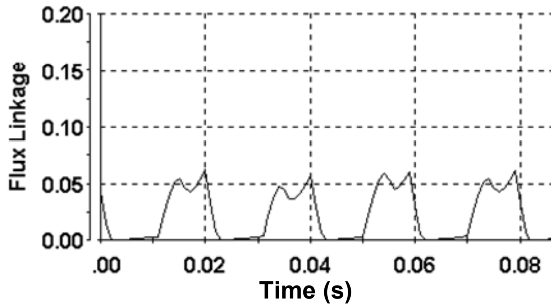

Figure 12. Experimental results of the estimated rotor flux

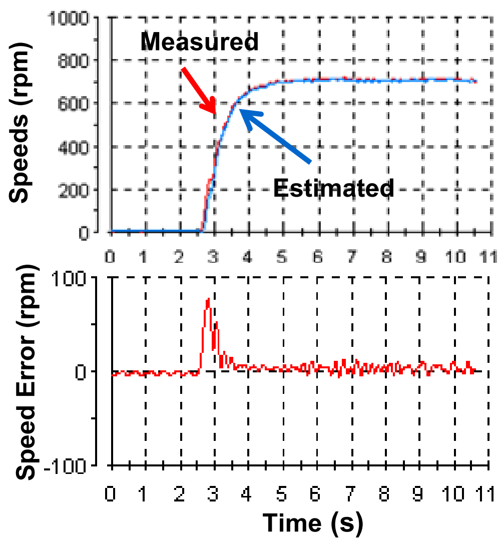

Figure 13. Experimental results of measured and estimated speeds as well as estimated speed error during starting operation at 700 rpm

VI. Conclusion

In this paper, a hybrid estimation technique for a wide speed range of a sensorless switched reluctance motor drive system has been proposed. The low frequency ramp method has been used for zero and very low speeds. The adaptive flux observer has been used for low, medium, and high speeds. The adaptive gains of adaptive flux observer have been designed based on Lyapunov theory. The proposed hybrid estimation technique has characterized by simplicity, low computation burden, no extra devices or circuits are required in compared with signal injection methods.

Different results have been presented to prove the accuracy and fast convergence of the proposed adaptive flux observer.

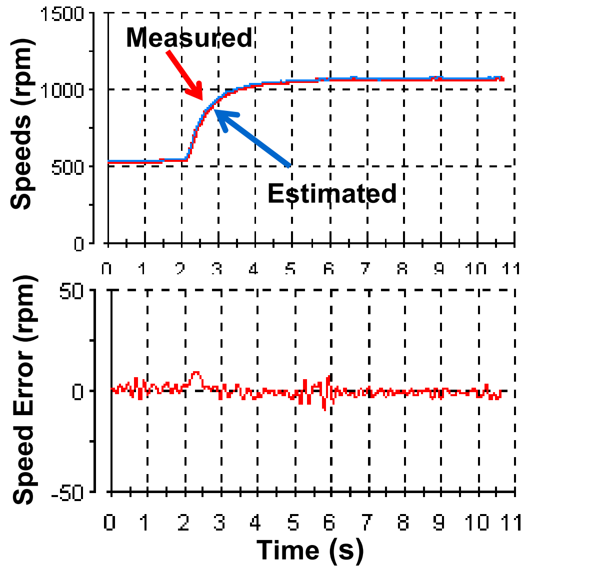

Figure 14. Experimental results of measured and estimated speeds as well as estimated speed error during step speed change from 550 rpm to 1100 rpm

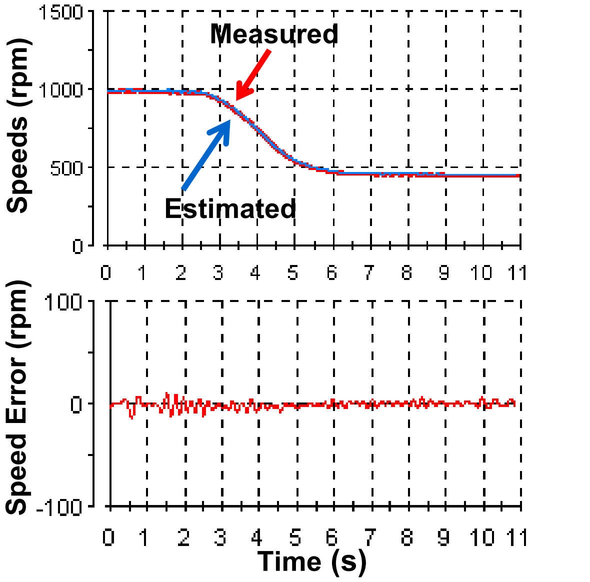

Figure 15. Experimental results of measured and estimated speeds as well as estimated speed error during step speed change from 1000 rpm to 450 rpm

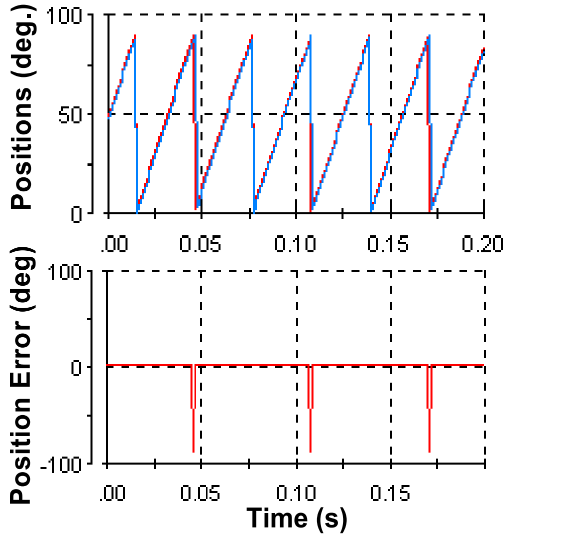

Figure 16. Experimental results of measured and estimated positions as well as estimated position error at speed of 500 rpm

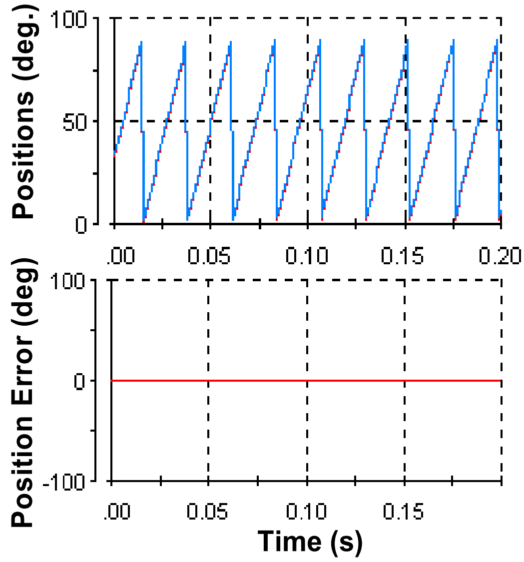

Figure 17. Experimental results of measured and estimated positions as well as estimated position error at speed of 700 rpm

APPENDIX

TABLE I. RATING AND DATA OF SRM

Item	Value
Power	375 W
Voltage	150 V
Current	2.5 A
Phase Resistance, Rph	8.6 Ω
L_u	0.035 H
Moment of inertia, J	0.01 kg.m^2
No of stator poles N_S	6
No of rotor poles N_r	4
No of phases q	3
Stator outer diameter D_o	146 mm
Stator inner diameter D	85.4 mm
Stator back iron width C	14.3 mm
Rotor outer diameter D_r	84.6 mm
Air gap length g	0.4 mm
Inter polar air gap length g_i	22.7 mm
Core axial length L_c	40.9 mm
Stator pole arc β_s	30°
Rotor pole arc β_r	45°
Shaft diameter d_{sh}	16 mm
No of turns /phase T_{ph}	560

TABLE II. COEFFICIENTS OF EQ. (6)

Item	Value
b_0	0.0156
b_1	0.174
b_2	0.6883

REFERENCES

[1] I. Husain, S. Hossain, "Modeling, simulation, and control of switched reluctance motor drives," IEEE Transactions on Industrial Electronics, vol. 52, no. 6, pp. 1625–1634, 2005. doi:10.1109/TIE.2005.858710

[2] K. Vijayakumar, R. Karthikeyan, S. Paramasivam, R. Arumugam, K. Srinivas, "Switched reluctance motor modeling, design, simulation, and analysis: a comprehensive review," IEEE Transactions on Magnetics, vol. 44, no. 12, pp. 4605–4617, 2008. doi:10.1109/TMAG.2008.2003334

[3] G. Lopez, P. Kjaer, T. Miller, "High-grade position estimation for SRM drives using flux linkage/current correction model," IEEE Transactions on Industry Applications, vol. 35, no. 4, pp. 859–869, 1999. doi:10.1109/28.777195

[4] J. Kim, R. Kim, "Online sensorless position estimation for switched reluctance motors using characteristics of overlap position based on inductance profile," IET Electrical Power Applications, vol. 13, no. 4, pp. 456-462, 2019. doi:10.1049/iet-epa.2018.5336

[5] D. Panda, V. Ramanarayanan, "Mutual coupling and its effect on steady-state performance and position estimation of even and odd number phase switched reluctance motor drive," IEEE Transactions on Magnetics, vol. 43, no. 8, pp. 3445-3456, 2007. doi:10.1109/TMAG.2007.898101

[6] S. Hossain, I. Husain, H. Klode, B. Lequesne, A. Omekanda, S. Gopalakrishnan, "Four-quadrant and zero-speed sensorless control of a switched reluctance motor", IEEE Transactions on Industry Applications, vol. 39, no. 5, pp. 1343-1349, 2003. doi:10.1109/TIA.2003.816541

[7] Y. Tang, Y. He1, F. Wang, D. Lee, J. Ahn, R. Kennel, "Back-EMF-based sensorless control system of hybrid SRM for high-speed operation," IET Electrical Power Applications, vol. 12, no. 6, pp. 867-873, 2018. doi:10.1049/iet-epa.2017.0641

[8] C. Gan, J. Wu, Y. Hu, S. Yang, W. Cao, J. Kirtley, "Online sensorless position estimation for switched reluctance motors using one current sensor," IEEE Transactions Power Electronics, vol. 31, no. 10, pp. 7248-7263, 2016. doi:10.1109/TPEL.2015.2505706

[9] M. Krishnamurthy, C. Edrington, B. Fahimi, "Prediction of rotor position at standstill and rotating shaft conditions in switched reluctance machines," IEEE Transactions Power Electronics, vol. 21, no. 1, pp. 255-263, 2006. doi:10.1109/TPEL.2005.861169

[10] S. Hossain, I. Husain, "A geometry based simplified analytical model of switched reluctance machines for real-time controller implementation," IEEE Transactions Power Electronics, vol. 18, no. 6, pp. 4605-4617, 2003. doi:10.1109/TPEL.2003.818870

[11] M. Islam, I. Husain, "Torque-ripple minimization with indirect position and speed sensing for switched reluctance motors," IEEE Transactions on Industrial Electronics, vol. 47, no. 5, pp. 1126–1133, 2000. doi:10.1109/41.873222

[12] L. Xu, C. Wang, "Accurate Rotor position detection and sensorless control of SRM for super-high operation," IEEE Transactions Power Electronics, vol. 17, no. 5, pp. 757-763, 2002. doi:10.1109/TPEL.2002.802196

[13] G. Pasquesoone, R. Mikail, I. Husain, "Position estimation at starting and lower speed in three-phase switched reluctance machines using pulse injection and two thresholds," IEEE Transactions on Industry Applications, vol. 47, no.4, pp. 1724-1731, 2011. doi:10.1109/TIA.2011.2156751

[14] H. Cheng, H. Chen, S. Xu, S. Yang, "Four-quadrant sensorless control in switched reluctance machine drive using pulse injection based on special flux linkage curves," IET Electrical Power Applications, vol. 11, no. 9, pp. 1566-1574, 2017. doi:10.1049/iet-epa.2017.0190

[15] J. Cai, Z. Deng, "Initial rotor position estimation and sensorless control of SRM based on coordinate transformation," IEEE Transactions Instrumentation and Measurement, vol. 64, no. 4, pp. 1004-1018, 2015. doi:10.1109/TIM.2014.2364699

[16] S. Paramasivam, S. Vijayan, M. Vasudevan, R. Arumugam, R. Krishnan, "Real-time verification of AI based rotor position estimation techniques for a 6/4 pole switched reluctance motor drive," IEEE Transactions on. Magnetics, vol. 43, no. 7, pp. 3209–3222, 2007. doi:10.1109/TMAG.2006.888811

[17] C. Hudson, N. Lobo, R. Krishnan, "Sensorless control of single switch-based switched reluctance motor drive using neural network," IEEE Transactions on Industrial Electronics, vol. 55, no. 1, pp. 321–329, 2008. doi:10.1109/TIE.2007.903965

[18] Y. Cai, Y. Wang, H. Xu, S. Sun, C. Wang, L. Sun, "Research on rotor position model for switched reluctance motor using neural network," IEEE/ASME Transactions of Mechatronics, vol. 23, no. 6, pp. 2762 - 2773, 2018. doi:10.1109/TMECH.2018.2870892

[19] N. Ertugrul, D. Cheok, "Indirect angle estimation in switched reluctance motor drives using fuzzy logic based motor model," IEEE Transactions Power Electronics, vol. 15, no. 6, pp. 1029–1044, 2000. doi:10.1109/63.892817

[20] E. Mese, D. Torrey, "An approach for sensorless position estimation for switched reluctance motors using artificial neural networks," IEEE Transactions Power Electronics, vol. 17, no. 1, pp. 66-75, 2002. doi:10.1109/63.988671

[21] E. Ofori, T. Husain, Y. Sozer, I. Husain, "A pulse-injection-based sensorless position estimation method for a switched reluctance machine over a wide speed range," IEEE Transactions on Industry Applications, vol. 51, no. 5, pp. 3867-3876, 2015.

[22] N. Chen, G. Cao, S. Huang, J. Sun, "Sensorless control of planar switched reluctance motors based on voltage injection combined with core-loss calculation," IEEE Transactions on Industrial Electronics, Oct. 2019. doi:10.1109/TIE.2019.2946539

[23] K. Hu, Y. Chen and C. Liaw, “A reversible position sensorless controlled switched-reluctance motor drive with adaptive and intuitive commutation tunings,” IEEE Transactions on Power Electronics, vol. 30, no. 7, pp. 3781 – 3793, 2015. doi:10.1109/TPEL.2014.2342877

[24] A. Khalil, I. Husain, S. Hossain, S. Gopalakrishnan, A. Omekanda, B. Lequesne, H. Klode, "A hybrid sensorless SRM drive with eight- and six-switch converter topologies," IEEE Transactions on Industry Applications, vol. 41, no. 6, pp. 1647–1655, 2005. doi:10.1109/TIA.2005.858304

[25] J. Bu, L. Xu, "Eliminating starting hesitation for reliable sensorless control of switched reluctance motors," IEEE Transactions on Industry Applications, vol. 37, no. 1, pp. 59–66, 2001. doi:10.1109/28.903127

[26] F. Barnard, W. Villet, M. Kamper, "Hybrid active-flux and arbitrary injection position sensorless control of reluctance synchronous machines," IEEE Transactions on Industry Applications, vol.51, no.5, pp.3899-3906, 2015. doi:10.1109/TIA.2015.2425802

[27] A. Khalil, S. Underwood, I. Husain, H. Klode, B. Lequesne, S. Gopalakrishnan, A. Omekanda, "Four-quadrant pulse injection and sliding-mode-observer-based sensorless operation of a switched reluctance machine over entire speed range including zero speed," IEEE Transactions on Industry Applications, vol. 43, no. 3, pp. 714-723, 2007. doi:10.1109/TIA.2007.895746

[28] F. Peng, J. Ye, A. Emadi, Y. Huang, "Position sensorless control of switched reluctance motor drives based on numerical method," IEEE Transactions on Industry Applications, vol. 53, no. 3, pp. 2159-2168, 2017. doi:10.1109/TIA.2017.2672523

[29] J. Kim, R. Kim,” Sensorless direct torque control using the inductance inflection point for a switched reluctance motor” IEEE Transactions on Industrial Electronics, vol. 65 , no. 12 , pp. 9336 – 9345, 2018. doi:10.1109/TIE.2018.2821632

[30] A. Xu, J. Chen, P. Ren , J. Zhu,” Position sensorless control of switched reluctance motor based on a linear inductance model with variable coefficients” IET Energy Systems Integration, vol. 1 , no. 3, pp. 210-217, 2019. doi:10.1049/iet-esi.2019.0041

[31] S. Kuai, S. Zhao, F. Heng, X. Cui, "Position sensorless technology of switched reluctance motor drives including mutual inductance," IET Electrical Power Applications, vol. 11, no. 6, pp. 1085-1094, 2017. doi:10.1049/iet-epa.2016.0490

[32] J. Cai, Z. Liu, Y. Zeng, "Aligned position estimation based fault-tolerant sensorless control strategy for SRM drives," IEEE Transactions Power Electronics, vol. 34, no. 8, pp. 7754-7762, 2019. doi:10.1109/TPEL.2018.2877779

[33] H. Abdel-Maksoud, M. M. Khater, and S. M.Shaaban, "Adaptive fuzzy logic PI control for switched reluctance motor based inductance model," International Journal of Intelligent Engineering and Systems, vol. 10, no. 4, pp 41-49, 2017. doi:10.22266/ijies2017.0831.05